Citation:
Huang, J., Zhang, B., and Zhu, W. (July 26, 2022). "Quasi-Periodic Solutions of a Damped Nonlinear Quasi-Periodic Mathieu Equation by the Incremental Harmonic Balance Method with Two Time Scales." ASME. J. Appl. Mech. doi: https://doi.org/10.1115/1.4055086

DOI:
https://doi.org/10.1115/1.4055086

Journal of Applied Mechanics. Received March 18, 2022;
Accepted manuscript posted July 13, 2022. doi:10.1115/1.4055086




# Quasi-Periodic Solutions of a Damped Nonlinear Quasi-Periodic Mathieu Equation by the Incremental Harmonic Balance Method with Two Time Scales

**J.L. Huang***
Department of Applied Mechanics and Engineering
Sun Yat-sen University
Guangzhou 510275
PR China
Email: huangjl@mail.sysu.edu.cn

**B.X. Zhang**
Department of Applied Mechanics and Engineering
Sun Yat-sen University
Guangzhou 510275
PR China

**W.D. Zhu**
Department of Mechanical Engineering
University of Maryland, Baltimore County
1000 Hilltop Circle, Baltimore, MD 21250
Email: wzhu@umbc.edu





## ABSTRACT

*Quasi-periodic (QP) solutions of a damped nonlinear QP Mathieu equation with cubic nonlinearity are investigated by using the incremental harmonic balance (IHB) method with two time scales. The damped nonlinear QP Mathieu equation contains two incommensurable harmonic excitation frequencies, one is a small frequency while the other nearly equals to twice the linear natural frequency. It is found that Fourier spectra of QP solutions of the equation consist of uniformly spaced sidebands due to cubic nonlinearity. The IHB method with two time scales, which relates to the two excitation frequencies, is adopted to trace solution curves of the equation in an automatical way and find all frequencies of solutions and their corresponding amplitudes. Effects of parametric excitation are studied in detail. Based on approximation of QP solutions by periodic solutions with a large period,*

*Corresponding author

*Floquet theory is used to study the stability of QP solutions. Three types of QP solutions can be obtained from the IHB method, which agree very well with results from numerical integration. However, the perturbation method using the double-step method of multiple scales (MMS) obtains only one type of QP solutions since the ratio of the small frequency to the linear natural frequency of the first reduced-modulation equation is nearly 1 in the second perturbation procedure, while the other two types of QP solutions from the IHB method do not need the ratio. Furthermore, the results from the double-step MMS are different from those from numerical integration and the IHB method.*

**Keywords:** quasi-periodic Mathieu equation, double-step method of multiple scales, incremental harmonic balance method with two time scales, sideband

## 1 INTRODUCTION

Consider Mathieu equation governed by the equation with periodically varying coefficients

$$\ddot{x} + (\delta + \epsilon \cos t)\, x = 0, \tag{1}$$

where an overdot denotes differentiation with respect to time $t$, and $\delta$ and $\epsilon$ are constant parameters. Mathieu equation appears in two ways in nonlinear vibration problems: (i) in systems in which there is parametric excitation, and (ii) in stability analysis of steady-state periodic solutions of nonlinear systems [1]. Examples of such Mathieu equation occur in many physics and engineering fields [2], such as resonant inertial sensors [3], parametric resonances in microelectromechanical systems [4], a vertically driven pendulum [5] and a physical pendulum [6], and a wind turbine blade [7, 8].

The vast literature on Mathieu equation and its applications up to 2018 has been reviewed by Kovacic et al. [9]. Several extensions of Mathieu equation from Eq. (1) have been considered in it. Esmailzadeh and Nakhaie-jazar [10] used Schauder's fixed-point theorem to provide the condition

region to obtain periodic response of Mathieu-Duffing equation

$$\ddot{x} + (\delta + \epsilon \cos t)\, x + \xi x^3 = 0, \tag{2}$$

where $\xi$ is a coefficient of the cubic nonlinear term. Ng and Rand [11] used a perturbation method, which is second-order averaging, to analyze bifurcations of Mathieu-Duffing equation. Kovacic and Cveticanin [12] applied the perturbation method by using the method of strained parameters to obtain transition curves of Mathieu-Duffing equation with strong cubic nonlinearity. Zounes and Rand [13] investigated transition curves of the quasi-periodic (QP) Mathieu equation

$$\ddot{x} + (\delta + \epsilon (\cos t + \cos \omega t))\, x = 0, \tag{3}$$

where $\omega$ is an irrational excitation frequency. Rand et al. [14] and Rand and Morrison [15] further studied transition curves of the equation with 2:2:1 and 2:1:1 resonances near the point $\delta = 0.25$, $\omega = 1$ and $\delta = 0.25, \omega = 0.5$, respectively. The 2:2:1 and 2:1:1 resonances are related to the natural frequency of an unforced equation and the two parametric excitation frequencies. For instance, near the point of the natural frequency of 0.5 and the two parametric excitation frequencies of 1.0, the three frequencies have nearly the ratio of 2:2:1; the 2:2:1 resonance can then occur. Sofroniou and Bishop [16] demonstrated periodic and QP routes to chaos of the QP Mathieu equation under given parameter conditions. Belhaq et al. [17, 18] developed a new perturbation method by using the double-step method of multiple scales (MMS) to analysis the damped nonlinear QP Mathieu equation

$$\ddot{x} + c\dot{x} + \left(\tilde{\omega}_0^2 + \alpha \cos(2\omega t) + \beta \cos(2\omega_d t)\right) x + \xi x^3 = 0, \tag{4}$$

where $c$ is the coefficient of damping, $\tilde{\omega}_0$ is the linear natural frequency, $\omega$ is the parametric exci-

tation frequency near $\tilde{\omega}_0$, $\omega_d$ is a small excitation frequency, and $\alpha$ and $\beta$ are parametric excitation magnitudes. The damped nonlinear QP Mathieu equation contains two harmonic excitation freuqencies - the parametric excitation frequency $\omega$ and small excitation frequency $\omega_d$, which are incommensurable. Zounes and Rand [19] used Lie transform with elliptic functions to investigate the global behavior of the undamped equation of Eq. (4). The same equation with 2:2:1 resonance was studied by Abouhazim et al. [20] using the double-step MMS. There are many studies on the dynamics of parametrically excited systems subject to multiple frequency excitations, such as transition to turbulence in fluid mechanics [21], quasi-periodic oscillations of a tower under turbulent wind flow [22], and response of a basilar membrane to two tone stimuli [23]. Another example mentioned in [24] is the dynamics of a ship; parametric excitation occurs when a ship sails in longitudinal waves. By assuming the vertical force due to sea waves as a periodic force, the equation of motion becomes Mathieu equation. However, sea waves are not periodic in nature; instead, they contain incommensurate frequencies. All these problems require a theoretical framework to understand their responses; unfortunately there is not an effective analytical method for analyzing nonlinear QP Mathieu equations. This motivates one to provide a semi-analytical method to obtain accurate solutions of the damped nonlinear QP Mathieu equation.

Recently, some authors of this work presented an incremental harmonic balance (IHB) method with two time scales [25] that was used to analyze QP motions of multiple-degree-of-freedom (DOF) nonlinear systems with internal resonances, and later extended it to calculate QP motions of a Van der Pol-Mathieu equation in [26], where the IHB method with two time scales was used to find all frequencies of responses and their corresponding amplitudes. As an extension of the previous work, the IHB method with two time scales is employed here to obtain all QP solutions of the damped nonlinear QP Mathieu equation in Eq. (4). While the double-step MMS [18] has an advantage to provide analytical results, it is only applicable to obtain QP solutions of Eq. (4) whose Fourier spectra include a few frequency components and a weakly nonlinear equation such as Eq. (4) with small parameters. Also, the double-step MMS obtains only one type of QP solutions of Eq. (4) that actually has three types of QP solutions as discussed in Sec. 4. The aim of this work is to obtain all QP solutions of the damped nonlinear QP Mathieu equation by

using the IHB method with two time scales, whose some solutions cannot be obtained from the double-step MMS. The corresponding Fourier spectra are calculated, which greatly facilitates the understanding of the behavior of the damped nonlinear QP Mathieu equation.

## 2 BRIEF DESCRIPTION OF THE DOUBLE-STEP MMS FOR QP SOLUTIONS

For comparison purposes, the double-step MMS, presented in [17, 18, 27] for obtaining approximate QP solutions of various systems is briefly discussed first. The idea of the double-step MMS, which consists of two procedural perturbation steps, is to introduce two small parameters $\varepsilon$ and $\mu$ with $0 < \varepsilon \ll \mu \ll 1$ to transform the original QP oscillator to an autonomous system by performing two reductions [17]. In the first reduced system, let $\tilde{c} = \varepsilon^2\tilde{\tilde{c}}$, $\alpha = \varepsilon\tilde{\alpha}$, $\beta = \mu\tilde{\beta}$, $\tilde{\beta} = \varepsilon^2\tilde{\tilde{\beta}}$, $\omega_d = \varepsilon\tilde{\omega}_d$, and $\xi = \varepsilon^2\tilde{\xi}$ so that the equation of the system has the form with a small parameter $\varepsilon$. Then $x$ can be expanded in powers of $\varepsilon$ as a function of multiple independent variables $T_m = \varepsilon^m t$ with $m = 0, 1, 2, \cdots, n$. Using the MMS, one can obtain the first reduced-modulation equations of amplitude $a$ and phase $\gamma$ in the polar form with a small parameter $\mu$ and the expression of the excitation frequency $\omega$ near the linear natural frequency $\tilde{\omega}_0$. In the second reduced system, introduce the variable changes $u = a\cos\gamma$ and $v = -a\sin\gamma$ to transform the equations of amplitude $a$ and phase $\gamma$ to the equivalent Cartesian form so that $u$ and $v$ are expanded in powers of $\mu$ as a function of multiple independent variables $T_m = \mu^m t$ with $m = 0, 1, 2, \cdots, n$. Then, using the MMS again, one can obtain the solutions of $u$ and $v$ and the expression of the excitation frequency $\omega_d$ near the linear natural frequency $\tilde{\omega}_{10}$ of the first reduced-modulation equations. Combining the two MMS procedures yields the QP solution in the form

$$\begin{aligned} x(t) = &\sum_{j_2=-4}^{4} A_{1,j_2}\cos\left(\omega t + j_2\omega_d t + \varphi_{1,j_2}\right) \\ &+ \sum_{j_2=-4}^{4} A_{2,j_2}\cos\left(3\omega t + j_2\omega_d t + \varphi_{3,j_2}\right). \end{aligned} \tag{5}$$

where $A_{1,j_2}$ and $A_{2,j_2}$ are amplitudes. The detailed procedure of the double-step MMS is documented in [17, 18, 27].

It is noted that all frequencies in the QP solution in Eq. (5) are linear combinations of the two incommensurate excitation frequencies $\omega$ and $\omega_d$ with $\omega \gg \omega_d$. The schematic diagram of Fourier spectrum of a QP solution from the double-step MMS is shown in Fig. 1, which has two sidebands surrounding the two frequencies $\omega$ and $3\omega$ that are referred to as carrier frequencies. It has two discrete spectral lines at the carrier frequencies $\omega$ and $3\omega$ , which are surrounded by uniformly spaced sidebands. Each of the two sidebands is spaced $\omega_d$ apart and consists of eight frequencies excluding the carrier frequencies.

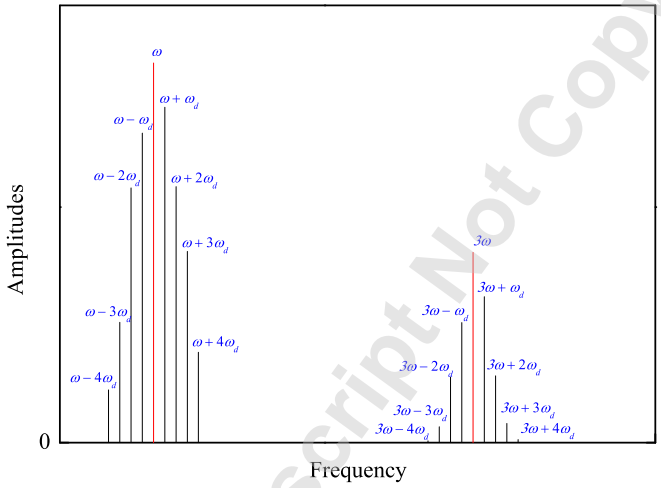


Fig. 1: Schematic diagram of the spectrum of a QP solution from the double-step MMS.

## 3 FORMULATION OF THE IHB METHOD WITH TWO TIME SCALES FOR QP SOLUTIONS

A general characteristic of quasi-periodic solutions whose Fourier spectra consist of uniformly spaced sidebands surrounding carrier frequencies was previously observed by Kreider and Nayfeh [28] from experimental investigation and was theoreitcally explained by some authors of this work [29]. Therefore, spectra of QP solutions contain the two excitation frequencies $\omega$ and $\omega_d$, where $\omega_d$ is the equal distance or its half between every two adjacent frequencies in sidebands as discussed in Sec. 4, and all frequencies of response are linear combinations of the two excitation frequencies. Following previous development by some authors of this work [25], one introduces two new time

variables defined as

$$\tau_1 = \omega t, \quad \tau_2 = \omega_d t \tag{6}$$

within the hyper-time domain $0 \leq \tau_1, \tau_2 \leq 2\pi$. Then $x(t)$ can be rewritten as a function of $\tau_1$ and $\tau_2$:

$$x(t) = x(\omega t, \omega_d t) = x(\tau_1, \tau_2) \tag{7}$$

Assume the following operator relations:

$$\begin{aligned} \Theta =& \frac{d}{dt} = \omega \frac{\partial}{\partial \tau_1} + \omega_d \frac{\partial}{\tau_2}, \\ \Theta^2 =& \frac{d^2}{d^2 t} = \omega^2 \frac{\partial^2}{\partial \tau_1^2} + 2\omega\omega_d \frac{\partial^2}{\partial \tau_1 \partial \tau_2} + \omega_d^2 \frac{\partial^2}{\partial \tau_2^2}. \end{aligned} \tag{8}$$

Substituting Eqs. (6) and (8) into Eq. (4) yields

$$\Theta^2 x + c\Theta x + \left(\tilde{\omega}_0^2 + \alpha \cos(2\tau_1) + \beta \cos(2\tau_2)\right) x + \gamma x^3 = 0, \tag{9}$$

The first step of the IHB method with two time scales is Newton-Raphson iterative procedure. Let ($x_0$, $\omega_0$, $\alpha_0$, $\omega_{d0}$, $\beta_0$) denote a guessed solution firstly; small increments are added to the guessed solution ($x_0$, $\omega_0$, $\alpha_0$, $\omega_{d0}$, $\beta_0$) to obtain a neighboring solution:

$$\begin{aligned} x =& x_0 + \Delta x, \quad \omega = \omega_0 + \Delta\omega, \quad \alpha = \alpha_0 + \Delta\alpha, \\ \omega_d =& \omega_{d0} + \Delta\omega_d, \quad \beta = \beta_0 + \Delta\beta. \end{aligned} \tag{10}$$

Substituting Eq. (10) into Eq. (9) and neglecting small increments of higher orders, one can obtain the linearized incremental equation

$$\begin{aligned}
&\Theta_0^2\Delta x + c\Theta_0\Delta x + \left(\tilde{\omega}_0^2 + \alpha_0\cos\left(2\tau_1\right) + \beta_0\cos\left(2\tau_2\right)\right)\Delta x \\
&\quad + 3\xi x_0^2\Delta x \\
&= R - \left[2\left(\omega_0\frac{\partial^2 x_0}{\partial\tau_1^2} + \omega_{d0}\frac{\partial^2 x_0}{\partial\tau_1\partial\tau_2}\right) + c\frac{\partial x_0}{\partial\tau_1}\right]\Delta\omega \\
&\quad - \left[2\left(\omega_{d0}\frac{\partial^2 x_0}{\partial\tau_2^2} + \omega_0\frac{\partial^2 x_0}{\partial\tau_1\partial\tau_2}\right) + c\frac{\partial x_0}{\partial\tau_2}\right]\Delta\omega_d \\
&\quad - x_0\cos\left(2\tau_1\right)\Delta\alpha - x_0\cos\left(2\tau_2\right)\Delta\beta,
\end{aligned} \tag{11}$$

where

$$\begin{aligned}
\Theta_0 &= \omega_0\frac{\partial}{\partial\tau_1} + \omega_{d0}\frac{\partial}{\tau_2}, \\
\Theta_0^2 &= \omega_0^2\frac{\partial^2}{\partial\tau_1^2} + 2\omega_0\omega_{d0}\frac{\partial^2}{\partial\tau_1\partial\tau_2} + \omega_{d0}^2\frac{\partial^2}{\partial\tau_2^2},
\end{aligned} \tag{12}$$

and

$$\begin{aligned}
R = -\big(&\Theta_0^2 x_0 + c\Theta_0 x_0 + \left(\tilde{\omega}_0^2 + \alpha_0\cos\left(2\tau_1\right)\right. \\
&\left.+\beta_0\cos\left(2\tau_2\right)\right)x_0 + \xi x_0^3\big)
\end{aligned} \tag{13}$$

is a correction term that would vanish if the current solution were exact.

The second step of the IHB method with two time scales is the Galerkin procedure. Under the effect of the nonlinear term between the two harmonic excitations, QP solutions of the damped nonlinear QP Mathieu equation can be obtained by expanding the displacement $x_0(\tau_1, \tau_2)$ in multiple Fourier series with finite terms in the hyper-time domain $0 < \tau_1, \tau_2 < 2\pi$ with $\tau_1 = \omega t$ and

$\tau_2 = \omega_d t$ and using the Galerkin procedure. One assumes

$$\begin{aligned} x_0 = &\sum_{j_1=1}^{2} \sum_{j_2=-N_m}^{N_m} a_{j_1,j_2} \cos\left((2j_1-1)\tau_1 + j_2\tau_2\right) \\ &+ \sum_{j_1=1}^{2} \sum_{j_2=-N_m}^{N_m} b_{j_1,j_2} \sin\left((2j_1-1)\tau_1 + j_2\tau_2\right), \end{aligned} \tag{14}$$

where $2N_m$ is the harmonic term numbers in a sideband, and $a_{j_1,j_2}$ and $b_{j_1,j_2}$ are Fourier coefficients. Spectra of QP solutions consist of sidebands, uniformly spaced with a distance of $\omega_d$ or $2\omega_d$, around the carrier frequencies $\omega$ and $3\omega$. Then all the frequency components of QP solutions of the damped nonlinear QP Mathieu equation can be expressed as $\omega, \omega \pm \omega_d, \omega \pm 2\omega_d, \cdots, \omega \pm m_1\omega_d, 3\omega, 3\omega \pm \omega_d, 3\omega \pm 2\omega_d, \cdots, 3\omega \pm m_2\omega_d$, where $m_1 \leq N_m$ and $m_2 \leq N_m$. Equation (14) can then be taken in the form

$$\begin{aligned} x_0 = &\sum_{j_2=-m_1}^{m_1} a_{1,j_2} \cos\left(\tau_1 + j_2\tau_2\right) + \sum_{j_2=-m_2}^{m_2} a_{2,j_2} \cos\left(3\tau_1 + j_2\tau_2\right) \\ &+ \sum_{j_2=-m_1}^{m_1} b_{1,j_2} \sin\left(\tau_1 + j_2\tau_2\right) + \sum_{j_2=-m_2}^{m_2} b_{2,j_2} \sin\left(3\tau_1 + j_2\tau_2\right) \\ = &\mathbf{C}_s\mathbf{A}, \end{aligned} \tag{15}$$

where

$$\begin{aligned} \mathbf{C}_s &= \left[\mathbf{C}_1\ \mathbf{C}_2\ \mathbf{S}_1\ \mathbf{S}_2\right], \\ \mathbf{A} &= \left[\mathbf{A}_1^{\mathrm{T}}\ \mathbf{A}_2^{\mathrm{T}}\ \mathbf{B}_1^{\mathrm{T}}\ \mathbf{B}_2^{\mathrm{T}}\right]^{\mathrm{T}}, \end{aligned} \tag{16}$$

in which

$$\begin{aligned}
\mathbf{C}_i &= \Big[\cos\left((2i-1)\tau_1 - m_i\tau_2\right)\cdots\ \cos\left((2i-1)\tau_1\right) \\
&\qquad \cdots\ \cos\left((2i-1)\tau_1 + m_i\tau_2\right)\Big], \\
\mathbf{S}_i &= \Big[\sin\left((2i-1)\tau_1 - m_i\tau_2\right)\cdots\ \sin\left((2i-1)\tau_1\right) \\
&\qquad \cdots\ \sin\left((2i-1)\tau_1 + m_i\tau_2\right)\Big], \\
\mathbf{A}_i &= \Big[a_{i,-m_i}\cdots\ a_{(2i-1),0}\cdots\ a_{(2i-1),m_i}\Big]^{\mathrm{T}} \\
\mathbf{B}_i &= \Big[b_{i,-m_i}\cdots\ b_{(2i-1),0}\cdots\ b_{(2i-1),m_i}\Big]^{\mathrm{T}}, \quad i = 1, 2.
\end{aligned} \tag{17}$$

The increment $\Delta x$ is expressed in the form

$$\Delta x = \mathbf{C}_s \Delta \mathbf{A}, \tag{18}$$

where $\Delta\mathbf{A} = \left[\Delta\mathbf{A}_1^{\mathrm{T}}\ \Delta\mathbf{A}_2^{\mathrm{T}}\ \Delta\mathbf{B}_1^{\mathrm{T}}\ \Delta\mathbf{B}_2^{\mathrm{T}}\right]^{\mathrm{T}}$. Substituting Eqs. (15) and (18) into Eq. (11) and applying Galerkin procedure to balance the harmonic terms yield

$$\begin{aligned}
&\int_0^{2\pi}\int_0^{2\pi} \delta(\Delta x)\left\{\Theta_0^2\Delta x + c\Theta_0\Delta x + \left[\tilde{\omega}_0^2 + \alpha_0\cos(2\tau_1)\right.\right. \\
&\quad \left.\left. + \beta_0\cos(2\tau_2)\right]\Delta x + 3\xi x_0^2\Delta x\right\} d\tau_1 d\tau_2 \\
&= \int_0^{2\pi}\int_0^{2\pi} \delta(\Delta x)\left\{R - \left[2\left(\omega_0\frac{\partial^2 x_0}{\partial\tau_1^2} + \omega_{d0}\frac{\partial^2 x_0}{\partial\tau_1\partial\tau_2}\right) + c\frac{\partial x_0}{\partial\tau_1}\right]\Delta\omega\right. \\
&\quad - \left[2\left(\omega_{d0}\frac{\partial^2 x_0}{\partial\tau_2^2} + \omega_0\frac{\partial^2 x_0}{\partial\tau_1\partial\tau_2}\right) + c\frac{\partial x_0}{\partial\tau_2}\right]\Delta\omega_d \\
&\quad \left. - x_0\cos(2\tau_1)\Delta\alpha - x_0\cos(2\tau_2)\Delta\beta\right\} d\tau_1 d\tau_2.
\end{aligned} \tag{19}$$

One can easily obtain a linear matrix in the form

$$\mathbf{K}_A \Delta \mathbf{A} = \mathbf{R} - \mathbf{R}_\omega \Delta\omega - \mathbf{R}_{\omega_d} \Delta\omega_d - \mathbf{R}_\alpha \Delta\alpha - \mathbf{R}_\beta \Delta\beta, \tag{20}$$

where

$$\begin{aligned}
\mathbf{K}_A &= \mathbf{M} + \mathbf{C} + \mathbf{K} + \mathbf{K}_\alpha + \mathbf{K}_\beta + 3\mathbf{K}_3, \\
\mathbf{R} &= -\left[\mathbf{M} + \mathbf{C} + \mathbf{K} + \mathbf{K}_\alpha + \mathbf{K}_\beta + \mathbf{K}_3\right]\mathbf{A}, \\
\mathbf{R}_\omega &= \left[2\mathbf{M}_\omega + \mathbf{C}_\omega\right]\mathbf{A},\ \mathbf{R}_{\omega_d} = \left[2\mathbf{M}_{\omega_d} + \mathbf{C}_{\omega_d}\right]\mathbf{A}, \\
\mathbf{R}_\alpha &= \int_0^{2\pi}\int_0^{2\pi} \cos\left(2\tau_1\right)\mathbf{C}_s^{\mathrm{T}}\mathbf{C}_s\mathbf{A}d\tau_1 d\tau_2, \\
\mathbf{R}_\beta &= \int_0^{2\pi}\int_0^{2\pi} \cos\left(2\tau_2\right)\mathbf{C}_s^{\mathrm{T}}\mathbf{C}_s\mathbf{A}d\tau_1 d\tau_2,
\end{aligned} \tag{21}$$

in which

$$\begin{aligned}
\mathbf{M} &= \int_0^{2\pi}\int_0^{2\pi} \mathbf{C}_s^{\mathrm{T}}\Theta_0^2\mathbf{C}_s d\tau_1 d\tau_2,\ \mathbf{C} = \int_0^{2\pi}\int_0^{2\pi} c\mathbf{C}_s^{\mathrm{T}}\Theta_0\mathbf{C}_s d\tau_1 d\tau_2, \\
\mathbf{K} &= \int_0^{2\pi}\int_0^{2\pi} \tilde{\omega}_0^2\mathbf{C}_s^{\mathrm{T}}\mathbf{C}_s d\tau_1 d\tau_2,\ \mathbf{K}_\alpha = \int_0^{2\pi}\int_0^{2\pi} \alpha_0\cos 2\tau_1\mathbf{C}_s^{\mathrm{T}}\mathbf{C}_s d\tau_1 d\tau_2, \\
\mathbf{K}_\beta &= \int_0^{2\pi}\int_0^{2\pi} \beta_0\cos 2\tau_2\mathbf{C}_s^{\mathrm{T}}\mathbf{C}_s d\tau_1 d\tau_2,\ \mathbf{K}_3 = \int_0^{2\pi}\int_0^{2\pi} \xi\mathbf{C}_s^{\mathrm{T}}\mathbf{C}_s\mathbf{A}\mathbf{C}_s\mathbf{A}\mathbf{C}_s d\tau_1 d\tau_2, \\
\mathbf{M}_\omega &= \int_0^{2\pi}\int_0^{2\pi} \mathbf{C}_s^{\mathrm{T}}\left(\omega_0\frac{\partial^2}{\partial\tau_1^2} + \omega_{d0}\frac{\partial^2}{\partial\tau_1\partial\tau_2}\right)\mathbf{C}_s d\tau_1 d\tau_2, \\
\mathbf{M}_{\omega_d} &= \int_0^{2\pi}\int_0^{2\pi} \mathbf{C}_s^{\mathrm{T}}\left(\omega_0\frac{\partial^2}{\partial\tau_1\partial\tau_2} + \omega_{d0}\frac{\partial^2}{\partial\tau_2^2}\right)\mathbf{C}_s d\tau_1 d\tau_2, \\
\mathbf{C}_\omega &= \int_0^{2\pi}\int_0^{2\pi} \cos\left(2\tau_1\right)\mathbf{C}_s^{\mathrm{T}}\mathbf{C}_s d\tau_1 d\tau_2,\ \mathbf{C}_{\omega_d} = \int_0^{2\pi}\int_0^{2\pi} \cos\left(2\tau_2\right)\mathbf{C}_s^{\mathrm{T}}\mathbf{C}_s d\tau_1 d\tau_2,
\end{aligned} \tag{22}$$

$\mathbf{K}_A$ is the tangent matrix, $\mathbf{R}$ is the corrective vector, and $\mathbf{R}_\omega$, $\mathbf{R}_{\omega_d}$, $\mathbf{R}_\alpha$, and $\mathbf{R}_\beta$ are vectors due to unit changes of $\Delta\omega$, $\Delta\omega_d$, $\Delta\alpha$, and $\Delta\beta$, respectively. The number of incremental unknowns

$(\Delta\mathbf{A}, \Delta\omega, \Delta\omega_d, \Delta\alpha, \Delta\beta)$ is greater than the number of equations in Eq. (20). If one wants to perform frequency response studies for a given excitation frequency $\omega_d$ and given constant parametric excitation magnitudes $\alpha$ and $\beta$, i.e., $\omega_d$, $\alpha$, and $\beta$ are fixed as constants, which implies $\Delta\omega_d = 0$, $\Delta\alpha = 0$, and $\Delta\beta = 0$, respectively, then Eq. (20) is reduced to

$$\mathbf{K}_A \Delta\mathbf{A} = \mathbf{R} - \mathbf{R}_\omega \Delta\omega. \tag{23}$$

The solution process starts from a proper known solution that can be a small amplitude solution, the iteration process is subsequently carried out with an updated correction vector $\mathbf{R}$ each time until the residue norm $|\mathbf{R}|$ is smaller than a permissible error for convergence, and the solution diagram of frequency response can then be easily traced by an increment $\Delta\omega$ or an increment of one component of $\mathbf{A}$. If one wants to perform parametric studies for, say $\beta$, for given excitation frequencies $\omega$ and $\omega_d$ and other constant parametric excitation magnitude $\alpha$, i.e., $\omega$, $\omega_d$, and $\alpha$ are fixed as constants, which implies $\Delta\omega = 0$, $\Delta\omega_d = 0$, and $\Delta\alpha = 0$, respectively, then Eq. (20) is reduced to

$$\mathbf{K}_A \Delta\mathbf{A} = \mathbf{R} - \mathbf{R}_\beta \Delta\beta. \tag{24}$$

In this case, the solution diagram of the parametric excitation magnitude $\beta$ can be easily traced by an increment $\Delta\beta$ or an increment of one component of $\mathbf{A}$.

### 3.1 Stability of QP solutions

Floquet theory extended to stability analysis of QP solutions in [30], which is based on approximation of QP solutions by periodic solutions, can be applied to study the stability of QP solutions in this work. One introduces a fundamental frequency defined as

$$\tilde{\omega} = \min\{|m\omega + n\omega_d| \,|\, m, n \in \mathcal{Z}\} \tag{25}$$

where $\tilde{\omega}$ is infinitely small, i.e., it is essentially 0, since the ratio of the two parametric excitation frequencies is incommensurable. However, when one approximates the ratio as a rational value, the fundamental frequency $\tilde{\omega}$ is a small value and nonzero. One can then assume

$$p_1 = \frac{\omega}{\tilde{\omega}},\ p_2 = \frac{\omega_d}{\tilde{\omega}},\ p_1, p_2 \in \mathcal{N}. \tag{26}$$

With approximation of the frequencies in Eq. (26), the displacement $x_0(\tau_1, \tau_2)$ in the multiple Fourier series in the form of Eq. (15) can be transferred to Fourier series in the form

$$\begin{aligned} x_0 = &\sum_{j_2=-m_1}^{m_1} a_{1,j_2} \cos(p_1 + j_2 p_2)\tau + \sum_{j_2=-m_2}^{m_2} a_{2,j_2} \cos(3p_1 + j_2 p_2)\tau \\ &+ \sum_{j_2=-m_1}^{m_1} b_{1,j_2} \sin(p_1 + j_2 p_2)\tau + \sum_{j_2=-m_2}^{m_2} b_{2,j_2} \sin(3p_1 + j_2 p_2)\tau, \end{aligned} \tag{27}$$

where $\tau = \tilde{\omega} t$. Then the stability of the periodic solution $x_0$ with a fundamental frequency $\tilde{\omega}$ can be investigated by superposing a small perturbation $\Delta x = s(t) e^{\lambda t}$ on the known $x_0$:

$$x = x_0 + \Delta x = x_0 + s(t) e^{\lambda t}, \tag{28}$$

where $s(t) = \tilde{\mathbf{C}}_s \tilde{\mathbf{U}}$, in which

$$\begin{aligned} \tilde{\mathbf{C}}_s = [&\cos(p_1 - m_1 p_2)\tilde{\omega}t \cdots \cos p_1 \tilde{\omega} t \cdots \cos(p_1 + m_1 p_2)\tilde{\omega}t \\ &\cos(3p_1 - m_1 p_2)\tilde{\omega}t \cdots \cos 3p_1 \tilde{\omega} t \cdots \cos(3p_1 + m_1 p_2)\tilde{\omega}t \\ &\sin(p_1 - m_1 p_2)\tilde{\omega}t \cdots \sin p_1 \tilde{\omega} t \cdots \sin(p_1 + m_1 p_2)\tilde{\omega}t \\ &\sin(3p_1 - m_1 p_2)\tilde{\omega}t \cdots \sin 3p_1 \tilde{\omega} t \cdots \sin(3p_1 + m_1 p_2)\tilde{\omega}t] \end{aligned} \tag{29}$$

and $\tilde{\mathbf{U}}$ is a nonzero vector of initial values, is a periodic term and $e^{\lambda t}$ is a decay term. Substituting Eq. (28) into Eq. (4), neglecting all the terms containing increment products, and noting that $x_0$ satisfies Eq. (4) yield

$$\Delta\ddot{x} + c\Delta\dot{x} + \left[\tilde{\omega}_0^2 + \alpha\cos\left(2p_1\tilde{\omega}t\right) + \beta\cos\left(2p_2\tilde{\omega}t\right) + 3\xi x_0^2\right]\Delta x = 0. \tag{30}$$

Differentiating $\Delta x$ with respect to time yields

$$\begin{aligned}\Delta\dot{x} &= \tilde{\omega}\tilde{\mathbf{C}}_s\tilde{\mathbf{U}}e^{\lambda t} + \lambda\tilde{\mathbf{C}}_s\tilde{\mathbf{U}}e^{\lambda t},\\ \Delta\ddot{x} &= \tilde{\omega}^2\tilde{\mathbf{C}}_s\tilde{\mathbf{U}}e^{\lambda t} + 2\lambda\tilde{\omega}\tilde{\mathbf{C}}_s\tilde{\mathbf{U}}e^{\lambda t} + \lambda^2\tilde{\mathbf{C}}_s\tilde{\mathbf{U}}e^{\lambda t}.\end{aligned} \tag{31}$$

Substituting Eqs. (31) and (15) into Eq. (30) yields

$$\begin{aligned}\Big(\lambda^2\tilde{\mathbf{C}}_s + 2\lambda\tilde{\omega}\tilde{\mathbf{C}}_s + \tilde{\omega}^2\tilde{\mathbf{C}}_s + \tilde{\omega}_0^2 + \alpha\cos\left(2p_1\tilde{\omega}t\right)\\ +\beta\cos\left(2p_2\tilde{\omega}t\right) + 3\xi\tilde{\mathbf{C}}_s\tilde{\mathbf{A}}\tilde{\mathbf{C}}_s\tilde{\mathbf{A}}\Big)\tilde{\mathbf{U}} = 0.\end{aligned} \tag{32}$$

Using Galerkin procedure as shown in Sec. 3 to balance the harmonic terms yields

$$\left(\lambda^2\tilde{\mathbf{M}} + \lambda\tilde{\mathbf{C}} + \tilde{\mathbf{K}}\right)\tilde{\mathbf{U}} = \mathbf{0}, \tag{33}$$

where

$$\tilde{\mathbf{M}} = \int_0^{2\pi} \tilde{\mathbf{C}}_s^{\mathrm{T}} \tilde{\mathbf{C}}_s d\tau, \tilde{\mathbf{C}} = \int_0^{2\pi} 2\tilde{\mathbf{C}}_s^{\mathrm{T}} \tilde{\mathbf{C}}_s' d\tau,$$
$$\tilde{\mathbf{K}} = \int_0^{2^\pi} \tilde{\mathbf{C}}_s^{\mathrm{T}} \left( \tilde{\mathbf{C}}_s'' + \tilde{\omega}_0^2 + \alpha \cos\left(2p_1\tau\right) \right.$$
$$\left. + \beta \cos\left(2p_2\tau\right) + 3\xi \tilde{\mathbf{C}}_s \mathbf{A} \tilde{\mathbf{C}}_s \mathbf{A} \right) d\tau. \tag{34}$$

The eigenvalue equation of Eq. (33) can be reformulated as

$$\mathbf{B}_1 \psi_k = \lambda_k \mathbf{B}_2 \psi_k, \tag{35}$$

where $\psi_k$ is the $k$th eigenvector associated with the eigenvalue $\lambda_k$ that represents Floquet exponents, and

$$\mathbf{B}_1 = \begin{bmatrix} \mathbf{0} & \mathbf{I} \\ -\tilde{\mathbf{K}} & \mathbf{0} \end{bmatrix}, \mathbf{B}_2 = \begin{bmatrix} \mathbf{I} & \mathbf{0} \\ \tilde{\mathbf{C}} & \tilde{\mathbf{M}} \end{bmatrix}. \tag{36}$$

According to Floquet theory, the stability criteria for QP solutions are related to Floquet exponents $\lambda_k$ that are the two eigenvalues with the smallest imaginary part in modulus [31, 30], with a negative real part indicating a stable solution as the perturbation $\Delta x$ decays with time, and a positive real part indicating an unstable solution.

## 4 NUMERICAL RESULTS AND DISCUSSION

QP solutions of the damped nonlinear QP Mathieu equation are investigated in this section. Parameters of the equation are similar to those in [18], with $c = 0.001$, $\tilde{\omega}_0^2 = 1.1$, $\alpha = 0.08$, $\omega = 1.2075$, $\omega_d = \sqrt{3}/20$, and $\gamma = 0.5$. To illustrate the power of the IHB method with two time scales, parametric excitation responses are investigated in detail here and the results are

compared with those from the double-step MMS as described in [17, 18] and numerical integration (NI) using the fourth-order Runge-Kutta (RK) method in the time domain and the fast Fourier transform to convert responses in the time domain to the frequency domain.

In the QP solution process of the IHB method with two time scales, the integer multiple $j_1$ of the first time scale $\tau_1$ is taken as $j_1 = 1, 3$. It is found that there exist three types of QP solutions related to integer multiples $j_2$ of the second time scale $\tau_2 = \omega_d t$, i.e., type I: $j_2 = \pm j$, type II: $j_2 = \pm 2j$, and type III: $j_2 = \pm(2j+1)$, where $j = 0, 1, 2, 3, \cdots$. Equation (15) can then be written as

$$\begin{aligned} x_0 = & \sum_{j_2=-m_1}^{m_1} A_{1,j_2} \cos\left(\tau_1 + j_2\tau_2 + \varphi_{1,j_2}\right) \\ & + \sum_{j_2=-m_2}^{m_2} A_{2,j_2} \cos\left(3\tau_1 + j_2\tau_2 + \varphi_{3,j_2}\right), \end{aligned} \tag{37}$$

where

$$A_{i,j_2} = \sqrt{a_{i,j_2}^2 + b_{i,j_2}^2}, \quad \varphi_{i,j_2} = \operatorname{atan2}\left(-b_{i,j_2}, a_{i,j_2}\right), \quad i = 1, 3, \tag{38}$$

in which $(m_1, m_2)$ are natural numbers, even positive integers, and odd positive integers for type I, type II, and type III, respectively. In other words, spectra of QP solutions in type I contain the carrier frequencies $(\omega, 3\omega)$ with uniformly spaced distance $\omega_d$ apart in sidebands; spectra of QP solutions in type II contain the carrier frequencies $(\omega, 3\omega)$ with uniformly spaced distance $2\omega_d$ apart in sidebands; and spectra of QP solutions in type III do not contain the frequencies $(\omega, 3\omega)$ with uniformly spaced distance $2\omega_d$ apart in sidebands. A noticeable and interesting feature of the damped nonlinear QP Mathieu equation, namely the presence of co-existing three types of QP solutions, is studied by using the IHB method with two time scales, while only type I QP solutions, but not type II or type III QP solutions, are obtained from the double-step MMS as discussed in Sec. 2.

### 4.1 Type I: spectra of QP solutions that contain the carrier frequencies $(\omega, 3\omega)$ with uniformly spaced distance $\omega_d$ apart in sidebands

The multiple Fourier series of Eq. (37) is used to continue the QP solution with uniformly spaced distance $\omega_d$ apart in sidebands and $m_1 = m_2 = 6$ so that with total harmonic terms retained $\tilde{n}_c = \tilde{n}_s = 2m_1 + 2m_2 + 2 = 26$. Figure 2 shows solution diagrams of the damped nonlinear QP Mathieu equation with $\omega = 1.2075$, $\omega_d = \sqrt{3}/20$, $c = 0.001$, $\tilde{\omega}_0 = 1.1$, $\alpha = 0.08$, and $\xi = 0.5$ from the three methods, i.e., the IHB method with two time scales, NI, and the double-step MMS, where amplitudes $A_{1,0}$, $A_{1,1}$, $A_{1,-1}$, $A_{1,2}$, and $A_{1,-2}$ defined in Eq. (37) correspond to the harmonic terms $\cos(\tau_1 + \varphi_{1,0})$, $\cos(\tau_1 + \tau_2 + \varphi_{1,1})$, $\cos(\tau_1 - \tau_2 + \varphi_{1,-1})$, $\cos(\tau_1 + 2\tau_2 + \varphi_{1,2})$, and $\cos(\tau_1 - 2\tau_2 + \varphi_{1,-2})$, respectively. The solutions of high-order harmonic terms are not shown here. It can be seen from Fig. 2 that the results from the IHB method with two time scales are nearly identical to those from NI for the whole range of the parametric excitation magnitude $\beta$, while the results from the double-step MMS show noticeable differences from the results from NI.

Presented in Fig. 2 are the QP response curves that exhibit two symmetric parts, where the parametric excitation magnitude $|\beta|$ ranges from 0.03436 to 0.10481 for the QP solutions from the IHB method with two time scales and NI and from $0.03436$ to $0.10481$ for the QP solutions from the double-step MMS. Amplitude $A_{1,0}$ corresponding to frequency $\omega$ in Fig. 2a is greater than other amplitudes in Figs. 2b-2e, i.e., the response is 2:1 resonance with parametric excitation frequency $2\omega$. In Figs. 2b and 2c, amplitudes $A_{1,1}$ and $A_{1,-1}$ start from zero when $|\beta| = 0.03436$ and terminate at zero when $|\beta| = 0.10481$ with peak points at $|\beta| = 0.06781$ and $|\beta| = 0.07233$, for the QP solutions from the IHB method with two time scales and NI. In other words, amplitudes $A_{1,1}$ and $A_{1,-1}$ along with $A_{1,\pm(2j+1)}$, where $j = 1, 2, 3, \cdots$, disappear when $|\beta|$ is out of the region $[0.03436,\ 0.10481]$, and amplitude $A_{1,0}$ along with $A_{1,\pm 2j}$ shifts to their corresponding amplitudes in the type II solution, as shown in Sec. 4.2, via two points at $|\beta| = 0.03436$ and $|\beta| = 0.10481$. This means that the two points at $|\beta| = 0.03436$ and $|\beta| = 0.10481$ are bifurcation points of the QP solution of the damped nonlinear QP Mathieu equation.

Presented in Fig. 3a are time histories with the parametric excitation magnitude $\beta = 0.04$ calculated by the three methods, i.e., the IHB method with two time scales, NI, and the double-

step MMS. The QP response is constructed by using NI with initial conditions $x_0(0) = 0.35527$ and $\dot{x}_0(0) = -0.85703$, which are obtained from the IHB method with two time scales at $t = 0$. The QP solution has two or more incommensurate frequencies, and since they are close to each other, the response exhibits a beating phenomenon as shown in Fig. 3a. Figure 3b shows the detailed response zone highlighted in Fig. 3a. To construct Poincaré section, one can rewrite Eq. (4) in the form of the four-dimensional system

$$\begin{cases} \dot{x}_1 &= x_2 \\ \dot{x}_2 &= -cx_2 - \left(\tilde{\omega}_0^2 + \alpha \sin 2\theta_1 + \beta \cos 2\theta_2\right) x - \gamma x^3 \\ \dot{\theta}_1 &= \omega_1 \\ \dot{\theta}_2 &= \omega_2 \end{cases}, \tag{39}$$

where $\theta_1 = \omega_1 t \pmod{2\pi}$ and $\theta_2 = \omega_2 t \pmod{2\pi}$. One can then obtain the global sections

$$\Sigma = \{(x_1, x_2, \theta_1, \theta_2) \in \mathcal{R}^1 \times \mathcal{R}^1 \times \mathcal{S}^1 \times \mathcal{S}^1 | \theta_1 = \theta_{10}\} \tag{40}$$

from the three methods shown in Fig. 3c, where $\mathcal{R}^n$ refers to an $n$-dimensional Euclidean space, $\theta_1$ and $\theta_2$ belong to the space $\mathcal{S}$, and $\theta_{10} \in [0, 2\pi)$ is a constant. The discrete points fall on the three closed curves corresponding to QP orbits. It can be seen from Fig. 3 that the result from the IHB method with two time scales agrees very well with that from NI, whereas the result from the double-step MMS shows noticeable deviations. In Fig. 3d, the corresponding spectra near the carrier frequency $\omega = 1.2075$, which is one of the basic frequencies, obtained from the three methods are shown, and there is a dominant peak at the carrier frequency $\omega = 1.2075$ with uniformly spaced sidebands surrounding it with the distance $\omega_d = \sqrt{3}/20$, which is the other basic frequency, between every two adjacent frequencies. Table 1 shows amplitudes of some harmonic

terms from the three methods as shown in Fig. 3d. It can also be seen from the table that the result from the IHB method with two time scales agrees very well with that from NI, whereas the result from the double-step MMS shows noticeable deviations.

Table 1: Values of amplitudes in Fig. 3d from the three methods, i.e., NI, the IHB method with two time scales, and the double-step MMS

| Amplitude | NI | IHB | MMS |
|---|---|---|---|
| $A_{1,-2}$ | 0.04359 | 0.04312 | 0.04567 |
| $A_{1,-1}$ | 0.02247 | 0.02209 | 0.12750 |
| $A_{1,0}$ | 0.86955 | 0.86964 | 0.77317 |
| $A_{1,1}$ | 0.04148 | 0.04048 | 0.29750 |
| $A_{1,2}$ | 0.05667 | 0.05622 | 0.05758 |

It should be noted that the accuracy of the IHB method with two time scales is related to harmonic numbers. The curves of $\beta \sim A_{1,0}$ obtained from the IHB method with two time scales are shown in Fig. 4a with different harmonic numbers $\tilde{n} = 4m_1 + 4m_2 + 4$ in Eq. (37), and the detailed solution curve zone highlighted there is shown in Fig. 4b. It can be seen that when the parametric excitation magnitude $\beta$ is small, i.e., $0.03436 \leq \beta < 0.08$, the curves of $\beta \sim A_{1,0}$ with different harmonic numbers are indistinguishable from each other; however, when the parametric excitation magnitude $\beta$ becomes large, i.e., $0.08 < \beta \leq 0.10481$, more harmonic numbers are required, i.e., $\tilde{n} = 60$ harmonic terms with $m_1 = m_2 = 7$, as shown in Fig. 4b, to yield a sufficiently accurate result. The CPU (AMD Ryzen 5 3500U (2.1GHz)) calculation time of an iteration with 60 harmonic terms is 0.16 s, which indicates the high efficiency of the IHB method with two time scale. Figure 5 shows Poincaré sections of the QP solution of the damped nonlinear QP Mathieu equation from NI and the IHB method with two time scales for different harmonic numbers when $\beta = 0.04$ and $\beta = 0.1033$. It can also be seen that when the parametric excitation magnitude $\beta$ is small, $\tilde{n} = 36$ harmonic terms with $m_1 = m_2 = 4$ yields a sufficiently accurate result, as shown in Fig. 5a. The QP solution from the IHB method with two time scales turns out to be sensitive to the harmonic number, as shown in Fig. 5b.

### 4.2 Type II: spectra of the QP solutions that contain the carrier frequencies $(\omega, 3\omega)$ with uniformly spaced distance $2\omega_d$ apart in sidebands

Spectra of the QP solutions in this case contain the carrier frequency $(\omega, 3\omega)$ with uniformly spaced distance $2\omega_d$ apart in sidebands; Eq. (37) can then be written as

$$\begin{aligned} x_0 =& A_{1,0}\cos(\tau_1+\varphi_{1,0}) + A_{1,\pm2}\cos(\tau_1\pm2\tau_2+\varphi_{1,\pm2}) \\ &+ A_{1,\pm4}\cos(\tau_1\pm4\tau_2+\varphi_{1,\pm4}) + \cdots \\ &+ A_{2,0}\cos(3\tau_1+\varphi_{3,0}) + A_{2,\pm2}\cos(3\tau_1\pm2\tau_2+\varphi_{3,\pm2}) \\ &+ A_{2,\pm4}\cos(3\tau_1\pm4\tau_2+\varphi_{3,\pm4}) + \cdots, \end{aligned} \tag{41}$$

Figure 6 shows the QP solution curves of amplitudes $A_{1,0}$, $A_{1,2}$, and $A_{1,-2}$ corresponding to the harmonic terms $\cos(\tau_1+\varphi_{1,0})$, $\cos(\tau_1+2\tau_2+\varphi_{1,2})$, and $\cos(\tau_1-2\tau_2+\varphi_{1,-2})$, respectively, versus the parametric excitation magnitude $\beta$ of the damped nonlinear QP Mathieu equation with $\omega = 1.2075$, $\omega_d = \sqrt{3}/20$, $c = 0.001$, $\tilde{\omega}_0 = 1.1$, $\alpha = 0.08$, and $\xi = 0.5$. The curves from the IHB method with two time scales have three closed parts. The green short dot lines represent type I QP response curves. It can be seen that the results from the IHB method with two time scales agree very well with those from NI. It is of interest to note that the response curves can shift between the type I solutions and type II solutions via the two bifurcation points at $|\beta| = 0.03436$ and $|\beta| = 0.10481$.

Figure 7 shows time histories, Poincaré sections, and spectra of the QP solution of the damped nonlinear QP Mathieu equation with $\omega = 1.2075$, $\omega_d = \sqrt{3}/20$, $c = 0.001$, $\tilde{\omega}_0 = 1.1$, $\alpha = 0.08$, and $\xi = 0.5$ at the parametric excitation magnitude $\beta = 0.6$ calculated by the IHB method with two time scales and NI. The QP response is constructed by using NI with initial conditions $x_0(0) = -0.63025$ and $\dot{x}_0(0) = -0.49874$, which are obtained from the IHB method with two time scales at $t = 0$. There is a dominant peak at the carrier frequency $\omega = 1.2075$ with uniformly spaced sidebands surrounding it with the distance $2\omega_d = \sqrt{3}/10$ between every two adjacent frequencies, as shown in Fig. 7c.

### 4.3 Type III: spectra of the QP solutions that do not have the frequencies $(\omega, 3\omega)$ with uniformly spaced distance $2\omega_d$ apart in sidebands

Spectra of the QP solutions in this case do not have the frequencies $(\omega, 3\omega)$ with uniformly spaced distance $2\omega_d$ apart in sidebands; Eq. (37) can then be written as

$$\begin{aligned} x_0 =& A_{1,\pm1}\cos\left(\tau_1 \pm \tau_2 + \varphi_{1,\pm1}\right) + A_{1,\pm3}\cos\left(\tau_1 \pm 3\tau_2 + \varphi_{1,\pm3}\right) \\ &+ A_{1,\pm5}\cos\left(\tau_1 \pm 5\tau_2 + \varphi_{1,\pm5}\right) + \cdots + A_{2,\pm1}\cos\left(3\tau_1 \pm \tau_2 + \varphi_{3,\pm1}\right) \\ &+ A_{2,\pm3}\cos\left(3\tau_1 \pm 3\tau_2 + \varphi_{3,\pm3}\right) + A_{2,\pm5}\cos\left(3\tau_1 \pm 5\tau_2 + \varphi_{3,\pm5}\right) + \cdots, \end{aligned} \tag{42}$$

Figure 8 shows the QP response curves of amplitudes $A_{1,-1}$, $A_{1,1}$, and $A_{1,3}$ corresponding to the harmonic terms $\cos\left(\tau_1 - \tau_2 + \varphi_{1,-1}\right)$, $\cos\left(\tau_1 + \tau_2 + \varphi_{1,1}\right)$, and $\cos\left(\tau_1 + 3\tau_2 + \varphi_{1,3}\right)$, respectively, versus the parametric excitation magnitude $\beta$ of the damped nonlinear QP Mathieu equation with $\omega = 1.2075$, $\omega_d = \sqrt{3}/20$, $c = 0.001$, $\tilde{\omega}_0 = 1.1$, $\alpha = 0.08$, and $\xi = 0.5$. The curves from the IHB method with two time scales have two closed parts. It can be seen that the results from the IHB method with two time scales agree very well with those from NI.

Figure 9 shows time histories, Poincaré sections, and spectra of the QP response of the damped nonlinear QP Mathieu equation with $\omega = 1.2075$, $\omega_d = \sqrt{3}/20$, $c = 0.001$, $\tilde{\omega}_0 = 1.1$, $\alpha = 0.08$, and $\xi = 0.5$ at the parametric excitation magnitude $\beta = 0.6$ calculated by the IHB method with two time scales and NI. The QP response is constructed by using NI with initial conditions $x_0(0) = 0.01751$ and $\dot{x}_0(0) = -0.67404$, which are obtained from the IHB method with two time scales at $t = 0$. There is a dominant peak at the frequency $\omega - \omega_d = 1.1209$ with uniformly spaced sidebands surrounding it with the distance $2\omega_d = \sqrt{3}/10$ between every two adjacent frequencies, as shown in Fig. 9c.

Note that NI is used to check the stability of QP solutions to verify that Floquet theory can be applied to conduct stability analysis of the damped nonlinear QP Mathieu equation based on approximation of QP solutions by periodic solutions with a large period. Time histories of quasi-periodic solutions obtained are shown in Figs. 3a, 7a, and 9a, respectively, which verify the stable solutions obtained from the IHB method with two time scales by using NI. The unstable solutions

obtained from the IHB method with two time scales exist in types II and III quasi-periodic solutions. NI can also be used to verify those unstable solutions. Figure 10 shows time histories of the quasi-periodic response at the parametric excitation magnitude $\beta = 0.4$ constructed by using NI with initial conditions $x_0(0) = -0.6638$ and $\dot{x}_0(0) = 0.0344$, which are obtained from the IHB method with two time scales at $t = 0$. It is interesting to find that the response of the damped nonlinear QP Mathieu equation jumps to the stable response of the type III solution after a finite time with starting from the unstable type II solution obtained from the IHB method with two time scales. The stability of all quasi-periodic solutions is checked a posteriori by using NI.

## 5 CONCLUSIONS

The IHB method with two time scales is an efficient, straightforward, and reliable method for treating the damped nonlinear QP Mathieu equation whose spectra contain sidebands, uniformly spaced with the distance $\omega_d$ or $2\omega_d$ apart, around the carrier frequencies $\omega$ and $3\omega$. Three types of QP solutions are obtained by using the present method. Based on approximation of QP solutions by periodic solutions with a large period, Floquet theory is applied to conduct stability analysis of the damped nonlinear QP Mathieu equation and accurately determine the bifurcation points. The accuracy of the present method is higher than that of the double-step MMS for the first type of QP solutions. The IHB method with two time scales can also be used to obtain the other two types of QP solutions, while the double-step MMS cannot be used to obtain these solutions. All the results from the IHB method with two time scales agree very well with those from NI using the fourth-order RK method even for moderately large values of the parametric excitation magnitude $\beta$ for the second and third types of QP solutions, which verifies that spectra of QP solutions of the damped nonlinear QP Mathieu equation contain uniformly spaced sidebands.

## ACKNOWLEDGEMENTS

Financial supports from the National Natural Science Foundation of China (Grant Nos. 11972381 and 11772100) and the Guangdong Basic and Applied Basic Research Foundation (Grant No. 2022A1515011809) are gratefully acknowledged.

## REFERENCES

[1] Rand, R. H., 2015, Lecture notes on nonlinear vibrations (version 53). see also url https://hdl.handle.net/1813/28989.

[2] Ruby, L., 1996, "Applications of the Mathieu equation," *American Journal of Physics,* **64**(1), Jan, pp. 39–44.

[3] Li, Y., Fan, S., Guo, Z., Li, J., Cao, L., and Zhuang, H., 2013, "Mathieu equation with application to analysis of dynamic characteristics of resonant inertial sensors," *Communications in Nonlinear Science and Numerical Simulation,* **18**(2), Feb, pp. 401–410.

[4] Turner, K. L., Miller, S. A., Hartwell, P. G., MacDonald, N. C., Strogatz, S. H., and Adams, S. G., 1998, "Five parametric resonances in a microelectromechanical system," *Nature,* **396**(6707), Nov, pp. 149–152.

[5] Raja, M. A. Z., Manzar, M. A., Shah, F. H., and Shah, F. H., 2018, "Intelligent computing for Mathieu's systems for parameter excitation, vertically driven pendulum and dusty plasma models," *Applied Soft Computing,* **62**, Jan, pp. 359–372.

[6] Fernandes, J. C., Sebastião, P. J., Gonçalves, L. N., and Ferraz, A., 2017, "Study of large-angle anharmonic oscillations of a physical pendulum using an acceleration sensor," *European Journal of Physics,* **38**(4), May, p. 045004.

[7] Ramakrishnan, V., and Feeny, B. F., 2012, "Resonances of a forced Mathieu equation with reference to wind turbine blades," *Journal of Vibration and Acoustics,* **134**(6), oct, p. 064501.

[8] Inoue, T., Ishida, Y., and Kiyohara, T., 2012, "Nonlinear vibration analysis of the wind turbine blade (occurrence of the superharmonic resonance in the out of plane vibration of the elastic blade)," *Journal of Vibration and Acoustics,* **134**(3), Apr, p. 031009.

[9] Kovacic, I., Rand, R., and Sah, S. M., 2018, "Mathieu's equation and its generalizations: Overview of stability charts and their features," *Applied Mechanics Reviews,* **70**(2), Feb, p. 020802.

[10] Esmailzadeh, E., and Nakhaie-jazar, G., 1997, "Periodic solution of a Mathieu-Duffing type equation," *International Journal of Non-Linear Mechanics,* **32**(5), Sep, pp. 905–912.

[11] Ng, L., and Rand, R., 2002, "Bifurcations in a Mathieu equation with cubic nonlinearities,"

*Chaos, Solitons & Fractals,* **14**(2), Aug, pp. 173–181.

[12] Kovacic, I., and Cveticanin, L., 2009, "The effects of strong cubic nonlinearity on the existence of periodic solutions of the Mathieu–Duffing equation," *Journal of Applied Mechanics,* **76**(5), Jun, p. 054501.

[13] Zounes, R. S., and Rand, R. H., 1998, "Transition curves for the quasi-periodic Mathieu equation," *SIAM Journal on Applied Mathematics,* **58**(4), Oct, pp. 1094–1115.

[14] Rand, R., Guennoun, K., and Belhaq, M., 2003, "2:2:1 resonance in the quasiperiodic Mathieu equation," *Nonlinear Dynamics,* **31**(4), pp. 367–374.

[15] Rand, R., and Morrison, T., 2005, "2:1:1 resonance in the quasi-periodic Mathieu equation," *Nonlinear Dynamics,* **40**(2), Apr, pp. 195–203.

[16] Sofroniou, A., and Bishop, S., 2014, "Dynamics of a parametrically excited system with two forcing terms," *Mathematics,* **2**(3), Sep, pp. 172–195.

[17] Belhaq, M., Guennoun, K., and Houssni, M., 2002, "Asymptotic solutions for a damped non-linear quasi-periodic Mathieu equation," *International Journal of Non-Linear Mechanics,* **37**(3), Apr, pp. 445–460.

[18] Guennoun, K., Houssni, M., and Belhaq, M., 2002, "Quasi-periodic solutions and stability for a weakly damped nonlinear quasi-periodic Mathieu equation," *Nonlinear Dynamics,* **27**(3), pp. 211–236.

[19] Zounes, R. S., and Rand, R. H., 2002, "Global behavior of a nonlinear quasiperiodic Mathieu equation," *Nonlinear Dynamics,* **27**(1), pp. 87–105.

[20] Abouhazim, N., Rand, R. H., and Belhaq, M., 2006, "The damped nonlinear quasiperiodic Mathieu equation near 2:2:1 resonance," *Nonlinear Dynamics,* **45**(3-4), Jun, pp. 237–247.

[21] Davis, S. H., and Rosenblat, S., 1980, "A quasiperiodic Mathieu–Hill equation," *SIAM Journal on Applied Mathematics,* **38**(1), feb, pp. 139–155.

[22] Luongo, A., and Zulli, D., 2011, "Parametric, external and self-excitation of a tower under turbulent wind flow," *Journal of Sound and Vibration,* **330**(13), jun, pp. 3057–3069.

[23] Robles, L., Ruggero, M. A., and Rich, N. C., 1997, "Two-tone distortion on the basilar membrane of the chinchilla cochlea," *Journal of Neurophysiology,* **77**(5), may, pp. 2385–2399.

[24] Sharma, A., and Sinha, S. C., 2018, "An approximate analysis of quasi-periodic systems via floquét theory," *Journal of Computational and Nonlinear Dynamics,* **13**(2), nov, p. 021008.

[25] Huang, J. L., and Zhu, W. D., 2017, "An incremental harmonic balance method with two timescales for quasiperiodic motion of nonlinear systems whose spectrum contains uniformly spaced sideband frequencies," *Nonlinear Dynamics,* **90**(2), Aug, pp. 1015–1033.

[26] Huang, J. L., Wang, T., and Zhu, W. D., 2021, "An incremental harmonic balance method with two time-scales for quasi-periodic responses of a Van der Pol–Mathieu equation," *International Journal of Non-Linear Mechanics,* **135**, p. 103767.

[27] Belhaq, M., and Houssni, M., 1999, "Quasi-periodic oscillations, chaos and suppression of chaos in a nonlinear oscillator driven by parametric and external excitations," *Nonlinear Dynamics,* **18**(1), pp. 1–24.

[28] Kreider, W., and Nayfeh, A. H., 1998, "Experimental investigation of single-mode responses in a fixed-fixed buckled beam," *Nonlinear Dynamics,* **15**(2), pp. 155–177.

[29] Huang, J. L., Xiao, L. J., and Zhu, W. D., 2020, "Investigation of quasi-periodic response of a buckled beam under harmonic base excitation with an "unexplained" sideband structure," *Nonlinear Dynamics,* **100**(3), may, pp. 2103–2119.

[30] Liao, H., Zhao, Q., and Fang, D., 2020, "The continuation and stability analysis methods for quasi-periodic solutions of nonlinear systems," *Nonlinear Dynamics,* **100**(2), pp. 1469–1496.

[31] Moore, G., 2005, "Floquet theory as a computational tool," *SIAM Journal on Numerical Analysis,* **42**(6), pp. 2522–2568.

## LIST OF FIGURES

## LIST OF TABLES

Journal of Applied Mechanics. Received March 18, 2022;
Accepted manuscript posted July 13, 2022. doi:10.1115/1.4055086



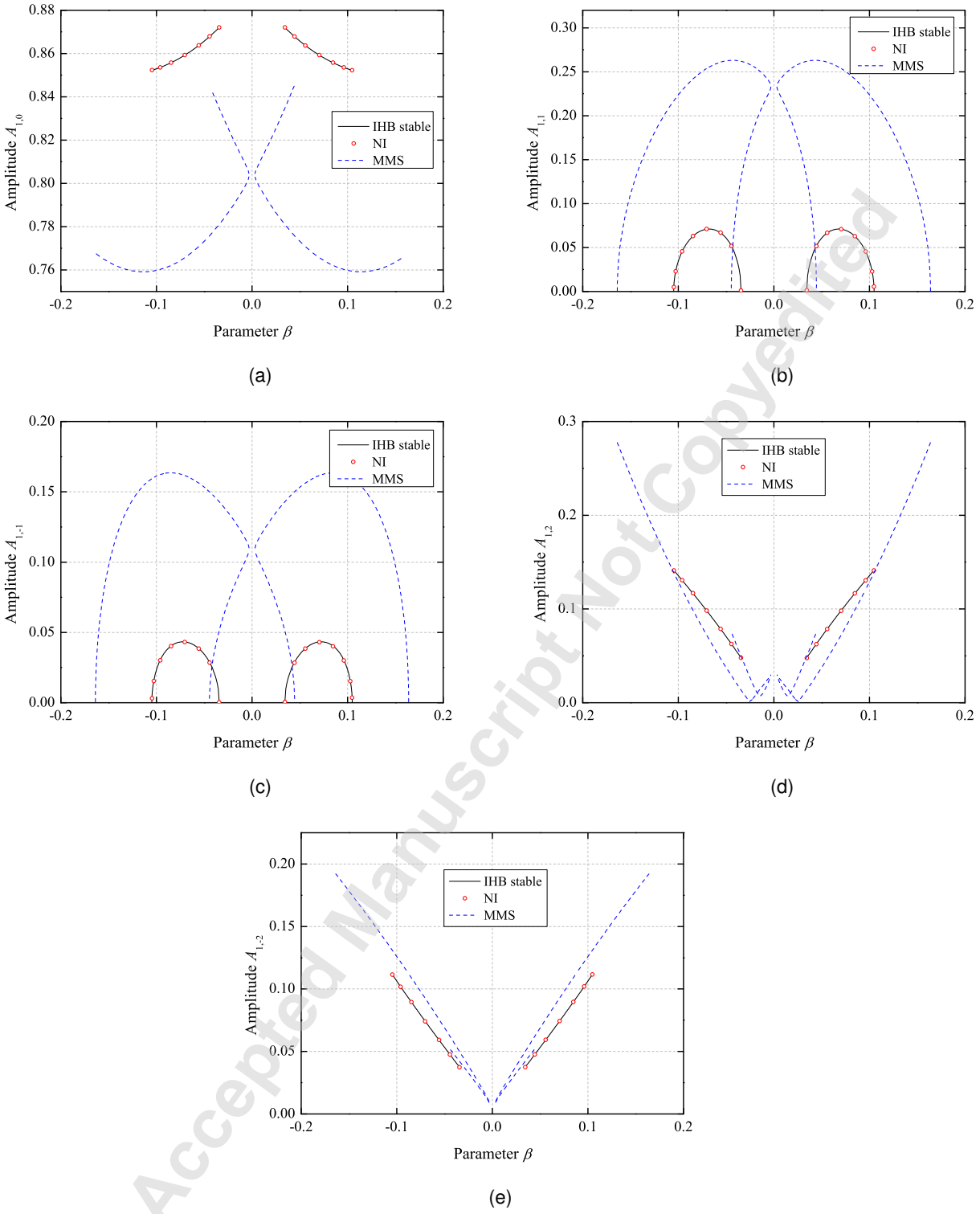


Fig. 2: Amplitudes of type I QP solutions of the damped nonlinear QP Mathieu equation versus the parametric excitation magnitude $\beta$ with $\omega = 1.2075$, $\omega_d = \sqrt{3}/20$, $c = 0.001$, $\tilde{\omega}_0 = 1.1$, $\alpha = 0.08$, and $\xi = 0.5$ from the three methods, i.e., the IHB method with two time scales, NI, and the double-step MMS: (a) $\beta \sim A_{1,0}$, (b) $\beta \sim A_{1,1}$, (c) $\beta \sim A_{1,-1}$, (d) $\beta \sim A_{1,2}$, and (e) $\beta \sim A_{1,-2}$.

Journal of Applied Mechanics. Received March 18, 2022;
Accepted manuscript posted July 13, 2022. doi:10.1115/1.4055086



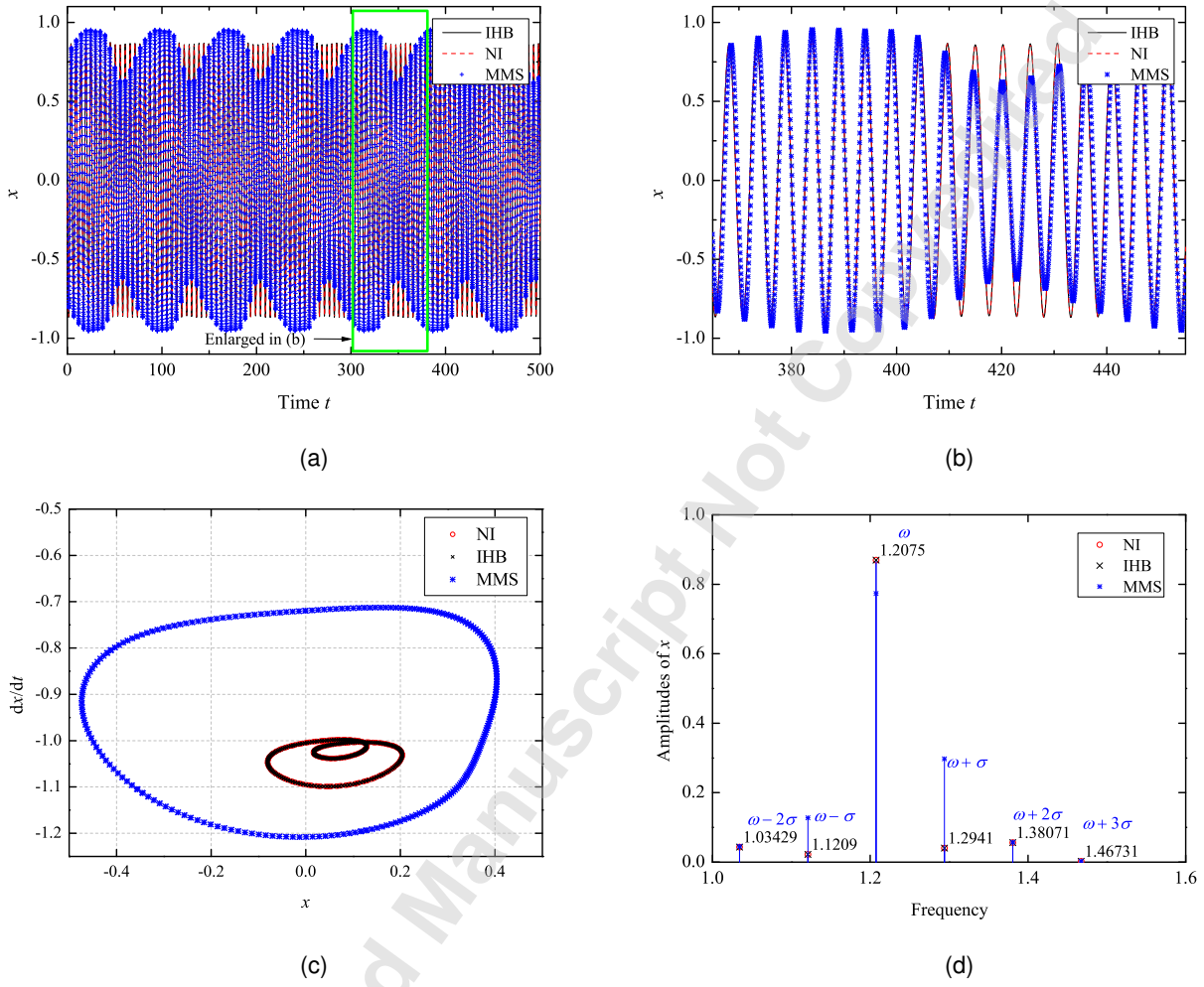


Fig. 3: IHB method with two time scales, NI, and the double-step MMS for type I QP solutions of the damped nonlinear QP Mathieu equation with $\omega = 1.2075$, $\omega_d = \sqrt{3}/20$, $c = 0.001$, $\tilde{\omega}_0 = 1.1$, $\alpha = 0.08$, and $\xi = 0.5$ at the parametric excitation magnitude $\beta = 0.04$: (a) time histories, (b) enlargement of a zone highlighted in (a), (c) Poincaré sections of the QP solutions, and (d) Fourier spectra.

Journal of Applied Mechanics. Received March 18, 2022;
Accepted manuscript posted July 13, 2022. doi:10.1115/1.4055086



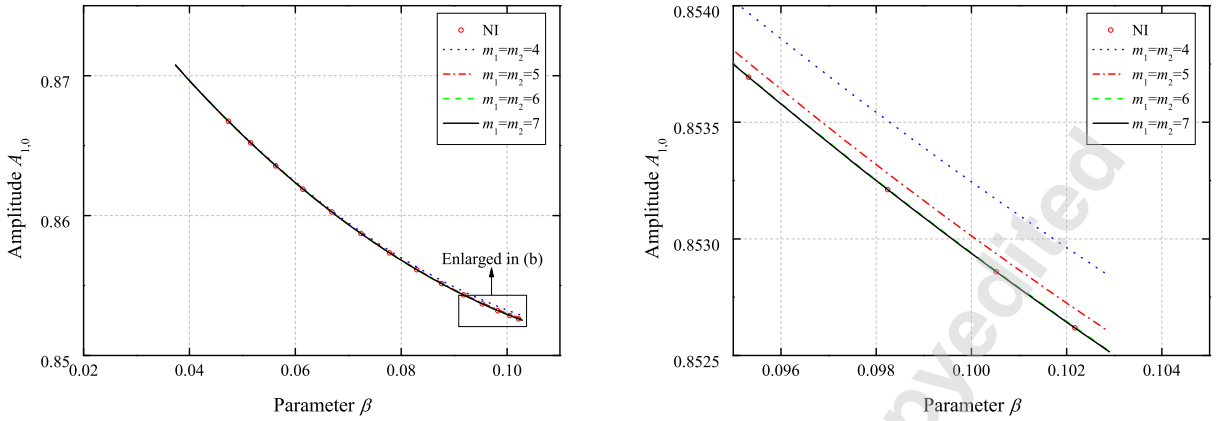


(a) (b)

Fig. 4: QP responses of the damped nonlinear QP Mathieu equation with $\omega = 1.2075$, $\omega_d = \sqrt{3}/20$, $c = 0.001$, $\tilde{\omega}_0 = 1.1$, $\alpha = 0.08$, and $\xi = 0.5$: (a) $\beta \sim A_{1,0}$, and (b) enlargement of a zone highlighted in (a).

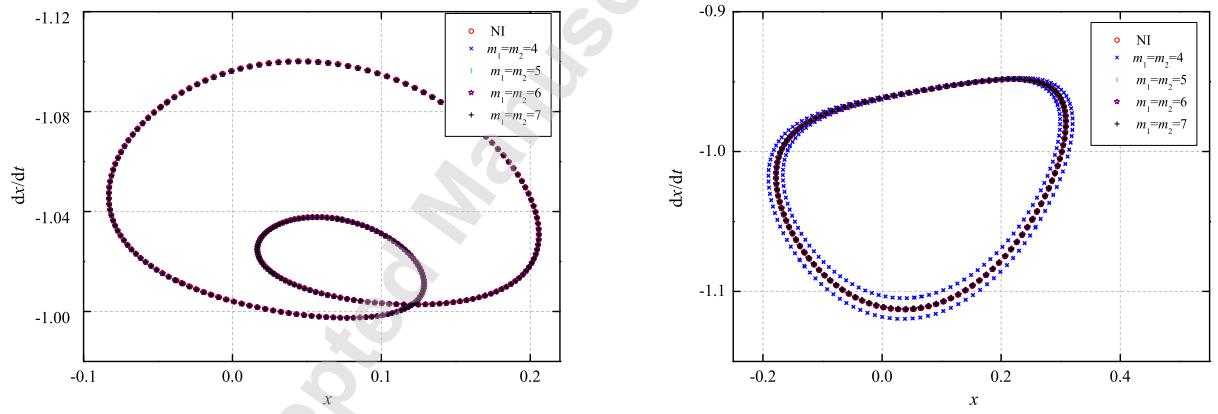


(a) (b)

Fig. 5: Poincaré sections of the QP responses of the damped nonlinear QP Mathieu equation with $\omega = 1.2075$, $\omega_d = \sqrt{3}/20$, $c = 0.001$, $\tilde{\omega}_0 = 1.1$, $\alpha = 0.08$, and $\xi = 0.5$ from NI and the IHB method with two time scales with different numbers of harmonic terms: (a) $\beta = 0.04$, and (b) $\beta = 0.1033$.

Journal of Applied Mechanics. Received March 18, 2022;
Accepted manuscript posted July 13, 2022. doi:10.1115/1.4055086



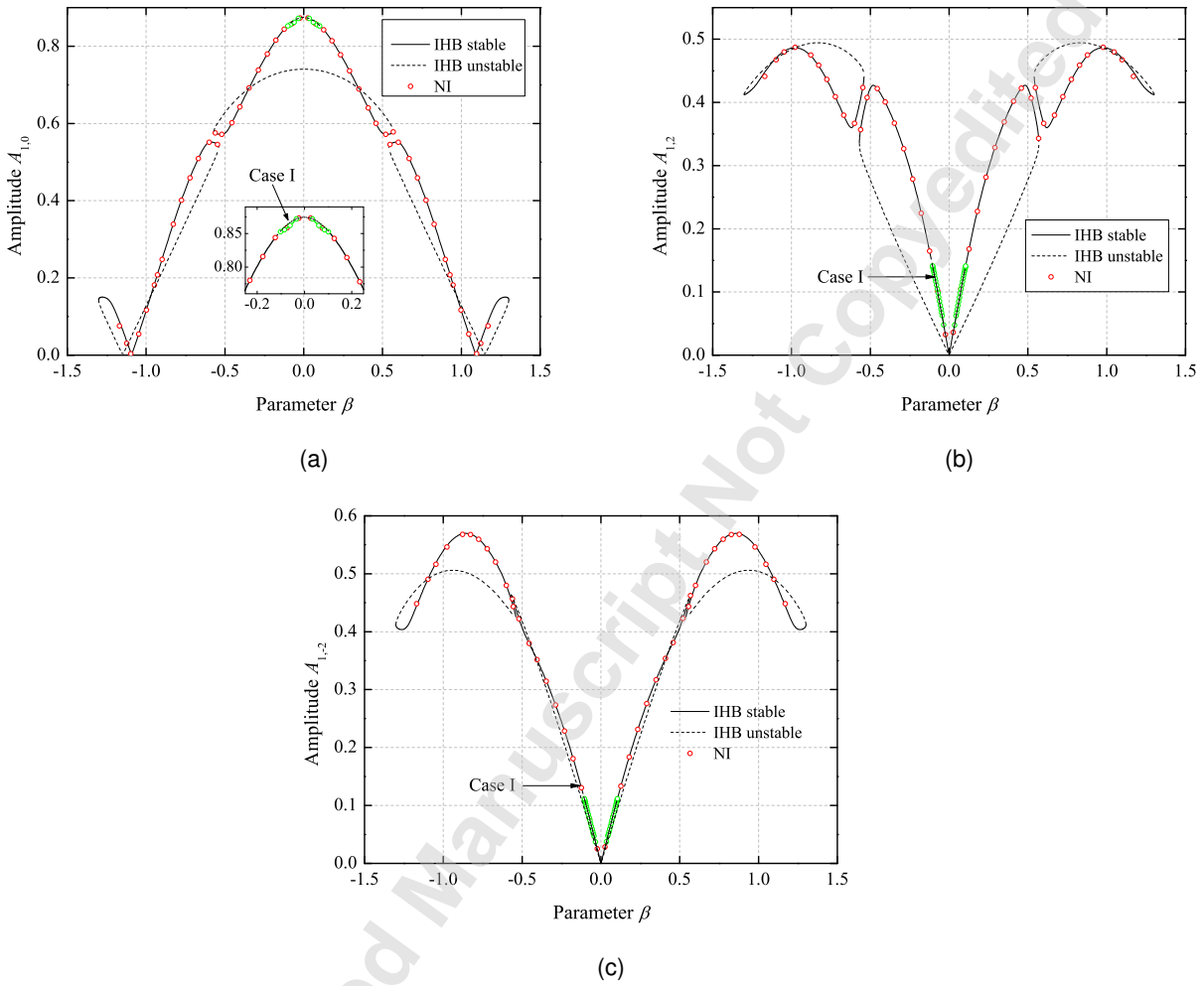


Fig. 6: Amplitudes of type II QP solutions versus the parametric excitation magnitude $\beta$ of the damped nonlinear QP Mathieu equation with $\omega = 1.2075$, $\omega_d = \sqrt{3}/20$, $c = 0.001$, $\tilde{\omega}_0 = 1.1$, $\alpha = 0.08$, and $\xi = 0.5$ from the IHB method with two time scales and NI; the QP solutions shown in green short dot lines are type I solutions: (a) $\beta \sim A_{1,0}$, (b) $\beta \sim A_{1,2}$, and (c) $\beta \sim A_{1,-2}$.

Journal of Applied Mechanics. Received March 18, 2022;
Accepted manuscript posted July 13, 2022. doi:10.1115/1.4055086



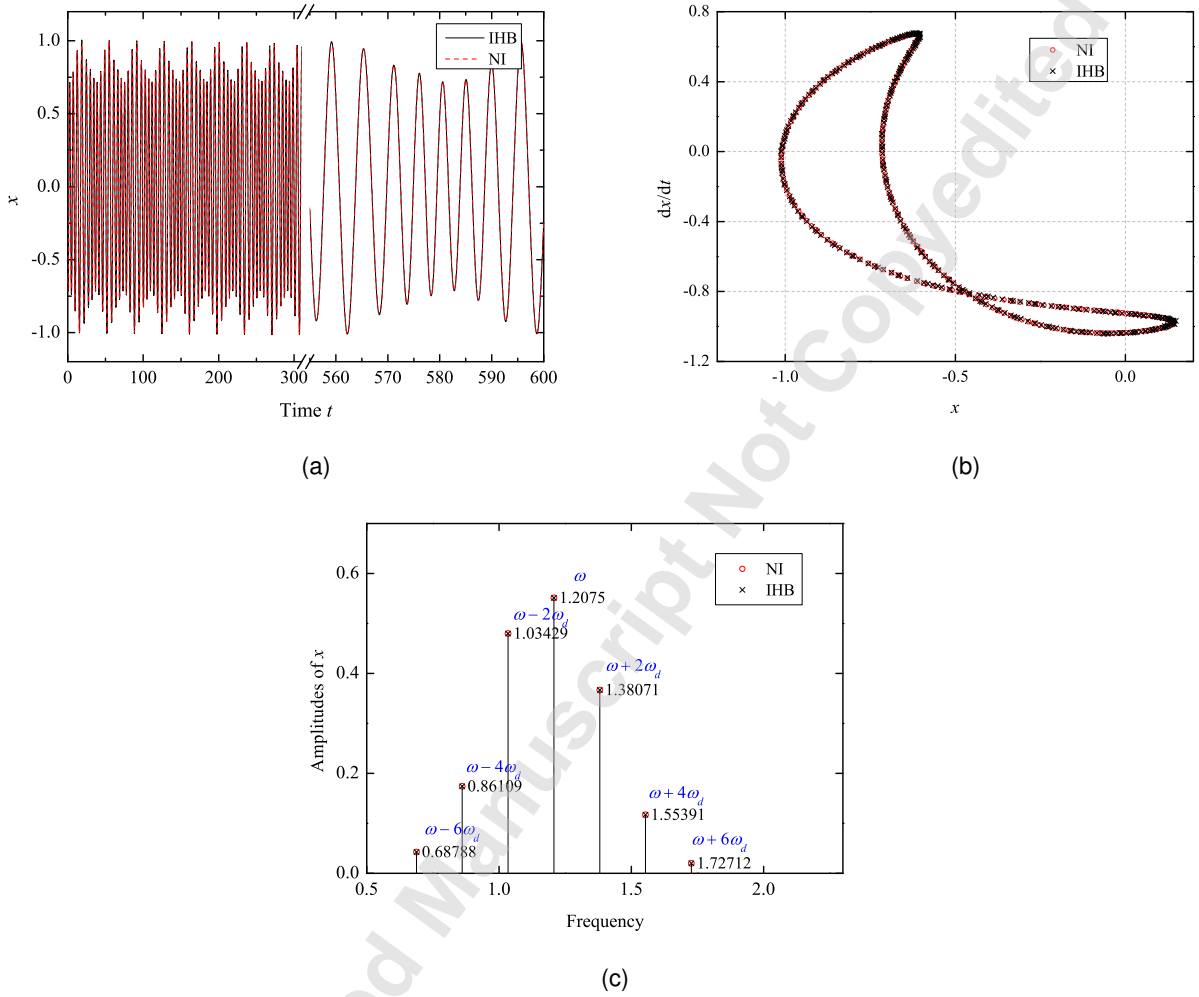


Fig. 7: IHB method with two time scales and NI for type II QP solutions of the damped nonlinear QP Mathieu equation with $\omega = 1.2075$, $\omega_d = \sqrt{3}/20$, $c = 0.001$, $\tilde{\omega}_0 = 1.1$, $\alpha = 0.08$, and $\xi = 0.5$ at the parametric excitation magnitude $\beta = 0.6$: (a) time histories, (b) Poincaré sections of the QP solutions, and (c) Fourier spectra.

Journal of Applied Mechanics. Received March 18, 2022;
Accepted manuscript posted July 13, 2022. doi:10.1115/1.4055086



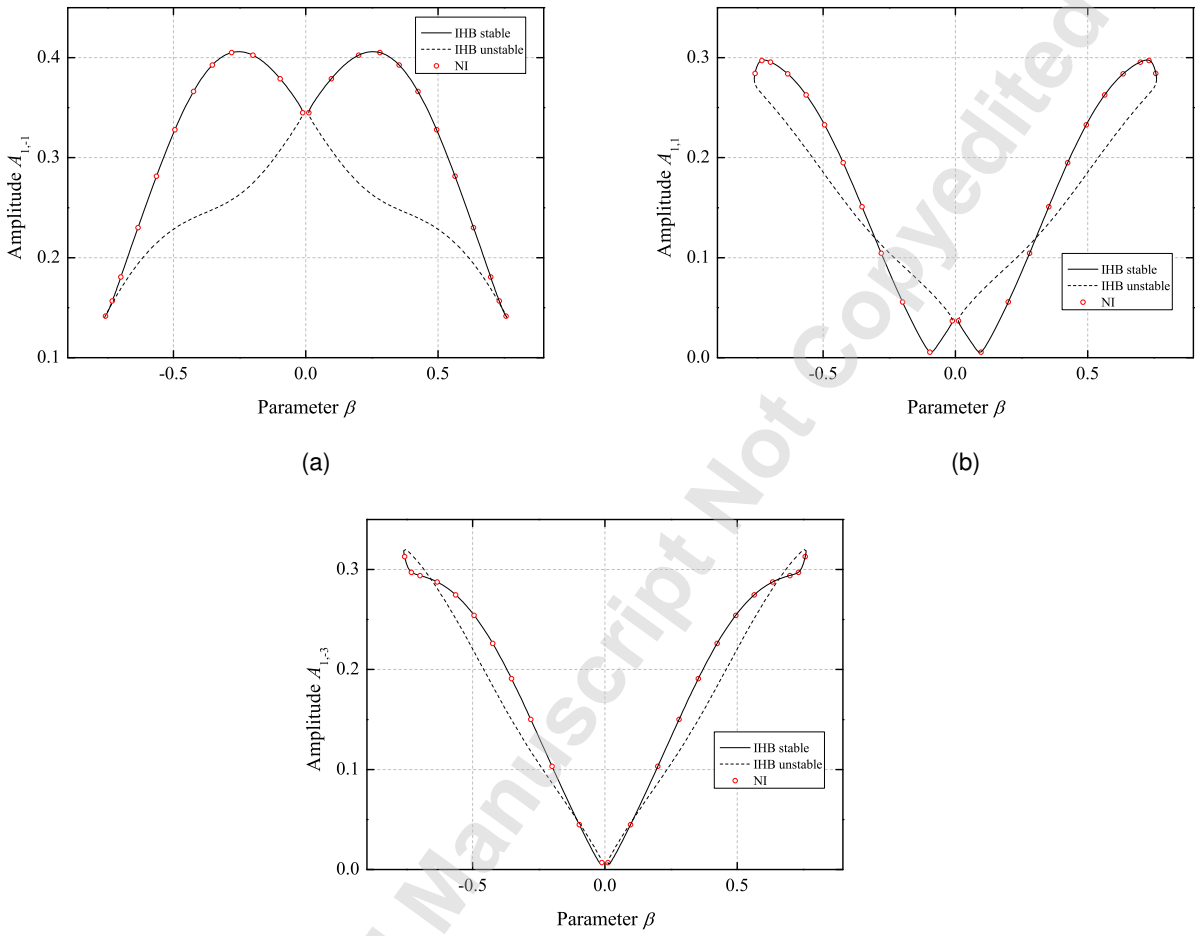


Fig. 8: Amplitudes of type III QP solutions versus the parametric excitation magnitude $\beta$ of the damped nonlinear QP Mathieu equation with $\omega = 1.2075$, $\omega_d = \sqrt{3}/20$, $c = 0.001$, $\tilde{\omega}_0 = 1.1$, $\alpha = 0.08$, and $\xi = 0.5$ from the IHB method with two time scales and NI: (a) $\beta \sim A_{1,-1}$, (b) $\beta \sim A_{1,1}$, and (c) $\beta \sim A_{1,-3}$.

Journal of Applied Mechanics. Received March 18, 2022;
Accepted manuscript posted July 13, 2022. doi:10.1115/1.4055086



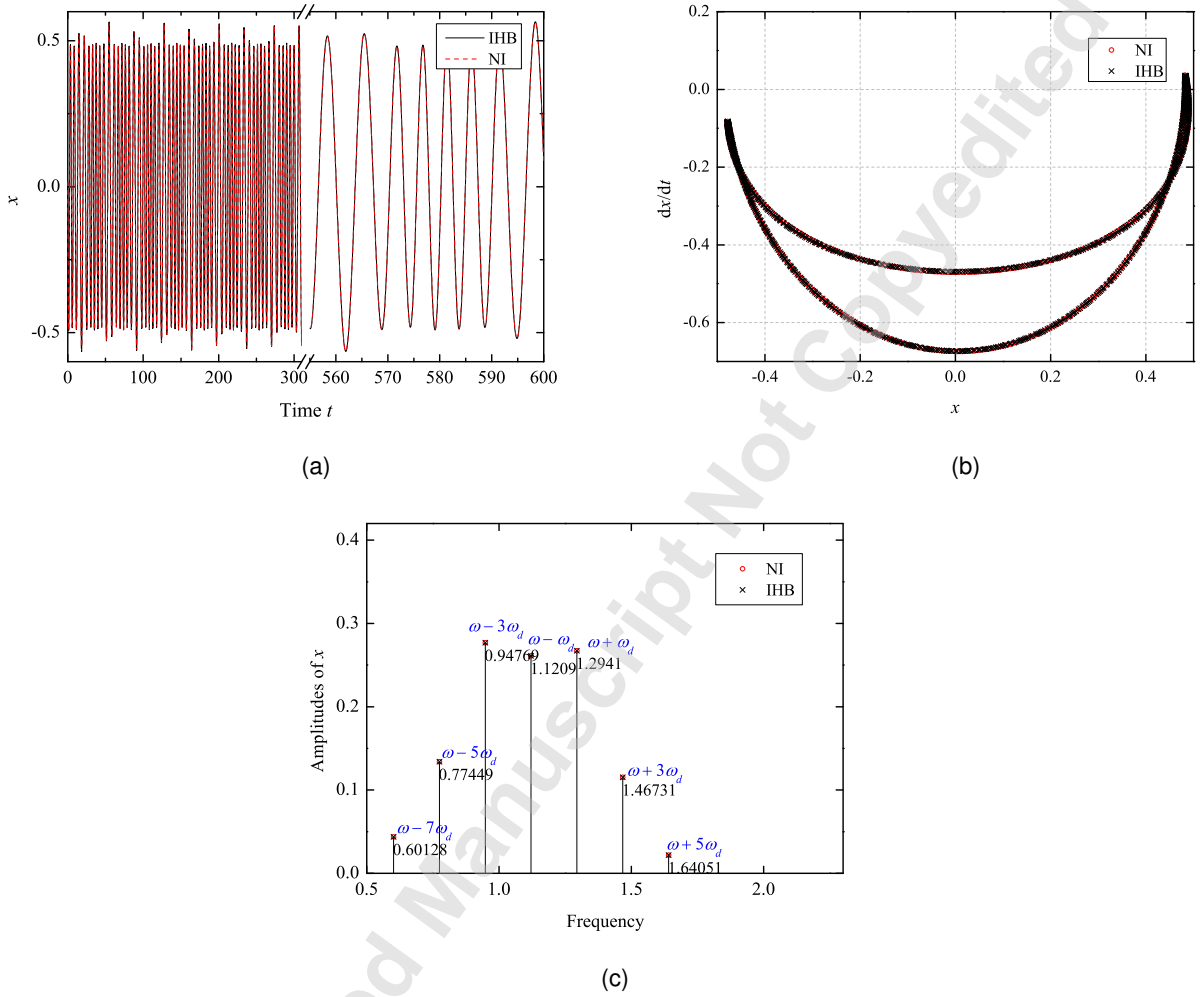


Fig. 9: The IHB method with two time scales and NI for type III QP solutions of the damped nonlinear QP Mathieu equation with $\omega = 1.2075$, $\omega_d = \sqrt{3}/20$, $c = 0.001$, $\tilde{\omega}_0 = 1.1$, $\alpha = 0.08$, and $\xi = 0.5$ at the parametric excitation magnitude $\beta = 0.6$: (a) time histories, (b) Poincaré sections of the QP solutions, and (c) Fourier spectra.

Journal of Applied Mechanics. Received March 18, 2022;
Accepted manuscript posted July 13, 2022. doi:10.1115/1.4055086



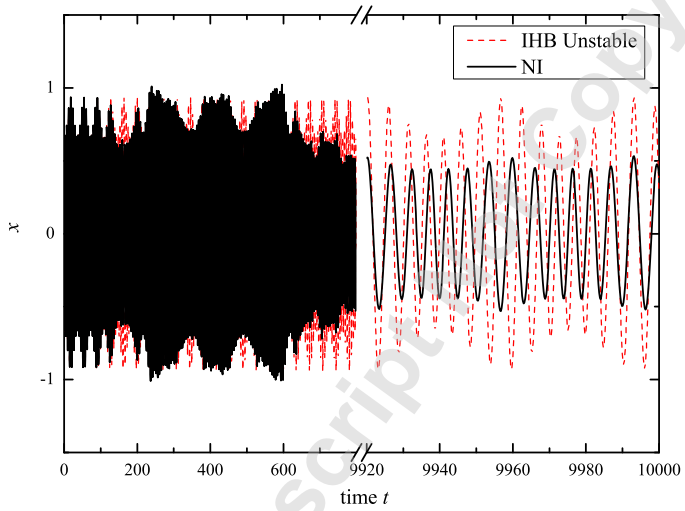


Fig. 10: Time histories of the damped nonlinear QP Mathieu equation with $\omega = 1.2075$, $\omega_d = \sqrt{3}/20$, $c = 0.001$, $\tilde{\omega}_0 = 1.1$, $\alpha = 0.08$, and $\xi = 0.5$ at the parametric excitation magnitude $\beta = 0.4$.